On the direct formation of HO2 radicals after 248 nm irradiation of benzene C6H6 in the presence of O2

ARTICLE *in* APPLIED PHYSICS B · SEPTEMBER 2008

Impact Factor: 1.86 · DOI: 10.1007/s00340-008-3065-8

CITATIONS
14

READS
36

4 AUTHORS:

Alina Aluculesei
Foundation for Research and Technology -…
9 PUBLICATIONS **73** CITATIONS
SEE PROFILE

Alexandre Tomas
Ecole des Mines de Douai
41 PUBLICATIONS **241** CITATIONS
SEE PROFILE

Coralie Schoemaecker
Université des Sciences et Technologies de …
51 PUBLICATIONS **295** CITATIONS
SEE PROFILE

Christa Fittschen
CNRS - Université Lille 1
113 PUBLICATIONS **1,353** CITATIONS
SEE PROFILE

Appl. Phys. B 92, 379–385 (2008)
DOI: 10.1007/s00340-008-3065-8

Applied Physics B
Lasers and Optics

A. ALUCULESEI[1]
A. TOMAS[2]
C. SCHOEMAECKER[1]
C. FITTSCHEN[1,✉]

On the direct formation of HO_2 radicals after 248 nm irradiation of benzene C_6H_6 in the presence of O_2

[1] Physicochimie des Processus de Combustion et de l'Atmosphère UMR, CNRS/USTL 8522, Université des Sciences et Technologies de Lille 1, 59655 Villeneuve d'Ascq Cedex, France
[2] Department of Chemistry and Environment, Ecole des Mines de Douai, 941 rue Charles Bourseul, 59508 Douai Cedex, France

Received: 15 January 2008/Revised version: 10 April 2008
Published online: 12 June 2008 •

ABSTRACT We present in this work the direct observation of HO_2 radicals after irradiation of benzene C_6H_6 at 248 nm in the presence of O_2. HO_2 radicals have been unambiguously identified using the very selective and sensitive detection of continuous wave cavity ring-down spectroscopy (cw-CRDS) coupled to a laser photolysis reactor. HO_2 radicals were detected in the first vibrational overtone of the OH stretch at 6638.20 cm^{-1}, using a DFB diode laser. This reaction might be important because 248 nm photolysis of H_2O_2 has often been used in the past for studying the $OH^\bullet$-initiated degradation of C_6H_6, often using a large excess of C_6H_6 over H_2O_2. The possible importance of the title reaction with respect to these former laboratory studies has been quantified through comparison with $HO_2^\bullet$ signals obtained from 248 nm photolysis of H_2O_2: one obtains under our conditions (excess O_2 and total pressure of 6.6 kPa helium) from the 248 nm irradiation of identical initial concentrations $[C_6H_6] = [H_2O_2]$ the following relative initial radical concentrations: $[HO_2^\bullet] = (0.28 \pm 0.05) \times [OH^\bullet]$. Experiments with various O_2 concentrations have revealed that the origin of the HO_2 radicals is not the reaction of H-atoms with O_2, but must originate from the reaction of O_2 with excited $C_6H_6{}^*$. The quantum yield of $C_6H_6{}^*$ formation has been deduced to $\varphi = 0.2 \pm 0.1$.

PACS 42.62.Fi; 82.20.Pm; 82.33.Tb

1 Introduction

Aromatic hydrocarbons, in particular the so-called BTX (benzene, toluene, xylene), are released in large amounts into the atmosphere. The major sources are anthropogenic such as automobile exhaust, solvent use, petrol evaporation and combustion including biomass burning. They contribute significantly to the photochemical formation of tropospheric ozone and other oxidants. Model calculations have shown that BTX can be the source of 30% of the photooxidant formation in urban areas [1]. But since the mechanism of tropospheric oxidation of aromatics is, despite many studies, still poorly resolved, the results of such calculations are not very reliable.

✉ Fax: +33-3-20337266, E-mail: christa.fittschen@univ-lille1.fr

The reaction with OH radicals is known to be the initial step in the atmospheric degradation of aromatics. In the case of benzene the addition, forming the hydroxycyclohexadienyl radical

$$C_6H_6 + OH^\bullet \rightleftharpoons C_6H_6{-}OH^\bullet$$

(hereafter referred to as adduct), is the only reaction of importance, abstraction leading to the formation of phenyl radicals and H_2O is negligible under atmospheric conditions. This reaction has been the subject of many experimental and theoretical studies [2–23] and its rate and equilibrium constants are obviously well established. Under tropospheric conditions the reverse reaction, i.e. the unimolecular decomposition of the adduct is negligible.

The reaction of this adduct with O_2, obviously an important reaction for atmospheric chemistry, has been intensively studied since then using different experimental techniques: excellent introductions into the state of knowledge have been given in recent publications on this subject [11, 12, 14, 18] and will not be repeated here. No consensus on the mechanism of this reaction has been found in these studies. Therefore we intended to use a new experimental technique, recently set-up in our laboratory, in order to shine some light from a new point of view onto this system: direct, absolute, time resolved, highly selective detection of $HO_2^\bullet$ is possible with our laser photolysis/cw-CRDS set-up. We intended to observe the rate of the possible formation of $HO_2^\bullet$ as well as its yield in the system $C_6H_6/OH^\bullet/O_2$. To our big surprise we observed already considerable amounts of $HO_2^\bullet$ by solely photolysing C_6H_6 in the presence of O_2, i.e. without any OH radicals in the system. Further investigation of this phenomena revealed that $HO_2^\bullet$ probably originates from a reaction between O_2 and excited C_6H_6 molecules rather than from a reaction between H-atoms and O_2.

While the 248 nm photolysis of C_6H_6 is of no direct interest for atmospheric chemistry, it might have an indirect influence: H_2O_2 photolysis at 248 nm has commonly been used [10, 12, 13, 24] to study the $OH^\bullet$ initiated oxidation of aromatic hydrocarbons. In order to prioritise the reaction of OH radicals with C_6H_6 rather than with H_2O_2 (both rate constants are very similar), C_6H_6 has always been used in excess, sometimes up to a factor of 6 [10]. Should there be a direct

formation of HO_2 radicals, and of course also a by-product, probably $C_6H_5^{\bullet}$, these radicals will influence the observed kinetics and product distributions, and must be taken into account when analyzing the concentration–time profiles.

2 Experimental technique

Two different detection techniques have been used in this work: cw-CRDS for HO_2 radicals and LIF for OH radicals.

2.1 *cw-CRDS*

The experimental setup has been described earlier [25–29], only a brief description is given here. The experimental set-up comprises three main components: the quasi-static reactor, the photolysis excimer laser (Lambda Physic LPX 202i) and the cw CRD spectrometer (see Fig. 1a).

A stainless steel flow cell was used as chemical reactor to enable the implementation of the cw-CRD spectrometer (cavity length 78 cm). The overlap between the probe laser beam and the photolysis laser beam was maximized to obtain the highest sensitivity; the length of the overlap region L_A was 37 cm. The near-infrared beam was provided by a fibered distributed feed-back (DFB) diode laser (Fitel-Furukawa) emitting up to 20 mW in the wavelength range $6640 \pm 13\,\mathrm{cm}^{-1}$.

The radiation is coupled into the cavity through a set of lenses and mirrors in order to obtain a good cavity mode matching to excite the fundamental TEM_{00} mode. The beam passes through an optical isolator and an acousto-optical modulator allowing to deviate the laser beam within 350 ns with respect to the trigger signal. The diode laser emission wavelength has been monitored using a fibered wavemeter (Burleigh WA-1100) with an accuracy of $0.01\,\mathrm{cm}^{-1}$. The optical signal transmitted through the cavity is converted into current by an avalanche effect photodiode (Perkin Elmer C30662E). A homemade amplifier-threshold circuit converts the current signal to an exploitable voltage signal and triggers the acquisition, i.e. the acousto-optical modulator, the delay generator (PAR 9650) and the digital oscilloscope (Tektronix TDS5052) that is used for data recording. The entire detection system has a bandwidth of 5 MHz. A personal computer is connected to the main devices either by GPIB or via a digital/analogic acquisition card (National Instruments PCI-6221). Control of the experiment and data acquisition and processing are executed by Labview 7.1 virtual instruments.

In order to extract the ring down times, the trigger signal and the output from the avalanche photodiode are recorded by the oscilloscope with 200 ns time resolution during 40 ms, starting 4 ms before the photolysis pulse permitting obtaining of one (sometimes two) ring down events before the photolysis pulse and several (two to six in general) ring down events after the photolysis pulse. After entirely transferring both traces to the computer, the positions of the individual ring-down events, and thus the delay with respect to the photolysis pulse, are first extracted from the trigger signal trace, the individual cavity ring-down decays are then sampled into a 160 μs time window, starting at each trigger signal. The ring down time is then roughly estimated by linear regression of the logarithmic decay and thereafter fitted over five lifetimes by a Levenberg-Marquardt Labview Virtual Instrument. Cavity mirrors with $R = 99.9967\%$ (Los Gatos) leading to typical decay times in the empty cell of 60 μs have been used.

All $HO_2^{\bullet}$ concentration–time profiles have been measured at peak of the most intense absorption line in the $2\nu_1$ band [27] at $6638.20\,\mathrm{cm}^{-1}$.

2.2 *LIF*

The OH radicals have been detected by laser induced fluorescence: a schematic view of the implementation of the LIF detection with respect to the cw-CRDS set-up is shown in Fig. 1b. OH radicals have been detected using a very common detection scheme: excitation is done in the (1,0) vibrational band in the A–X electronic transition at 282 nm, followed by a detection of the red-shifted fluorescence in the (1, 1) vibrational band around 308 nm. The excitation beam at 282 nm is delivered by a frequency doubled dye laser (Quantel TDL50), pumped by a frequency doubled YAG (Quantel YG780), using Rhodamin 590 as dye. The excitation beam propagates perpendicular to the photolysis beam, the fluorescence is collected through two lenses and an interference filter (308 ± 10 nm) and quantified by a photomultiplier, installed perpendicular to the laser beam plan. The fluorescence signal is integrated and averaged in a boxcar (EG&G 4121B). The analogue signal is then treated by an A/D-converter and transferred to a computer. A typical decay consists of 20–50 points at different delays between the two lasers, each averaged over typically 30 laser shots. Different delays between the pump and probe laser are realized by a digital delay generator (EG&G 9650), which is computer controlled.

All experiments have been performed at a total pressure of 6.6 kPa, typical total gas flows are $250\,\mathrm{cm}^3\,\mathrm{min}^{-1}$, leading to a flow velocity within the reactor of $2\,\mathrm{cm\,s}^{-1}$. The different gases were introduced into the cavity as stabilized flow using calibrated flow controllers (Tylan FC-260). The total pressure was kept constant using the pressure controller (Leybold-Heraeus MR 16) installed at the exit of the reactor. Typical concentrations were $[C_6H_6] = 0.6\text{–}3 \times 10^{15}\,\mathrm{cm}^{-3}$, $[H_2O_2] = 5 \times 10^{14}\,\mathrm{cm}^{-3}$ and $[O_2] = 1.5 \times 10^{17}\,\mathrm{cm}^{-3}$. C_6H_6 was prepared manometrically as diluted mixtures (typically 3%–5%) in 10 l glass balloons.

The repetition rate has been 0.2 Hz in CRDS-Experiments, limited by the time necessary to handle the data acquisition. A few experiments have been performed with an even lower repetition rate (0.1 Hz), no influence on the $HO_2^{\bullet}$ profiles has been observed. We therefore believe that this repetition rate permits a sufficient renewal of the reaction mixture between two photolysis laser shots even though photolysis occurs along the axis of the gas flow (see Fig. 1a). The gas mixture is not only renewed by the gas flow, but also from diffusion: the photolysed volume represents less than 10% of the total volume. In the case of LIF experiments the repetition rate has to be 10 Hz for two reasons: (1) the YAG laser needs to operate at 10 Hz in order to be stable and (2) a large number of fluorescence signals has to be averaged at any given delay. At this repetition rate a renewal of the gas mixture can not be ensured with the photolysis axis parallel to the gas flow, we therefore reduce the size of the photolysis beam ($1 \times 1\,\mathrm{cm}^2$ instead of $3.5 \times 1\,\mathrm{cm}^2$ in the case of cw-CRDS) and enter it perpendicu-

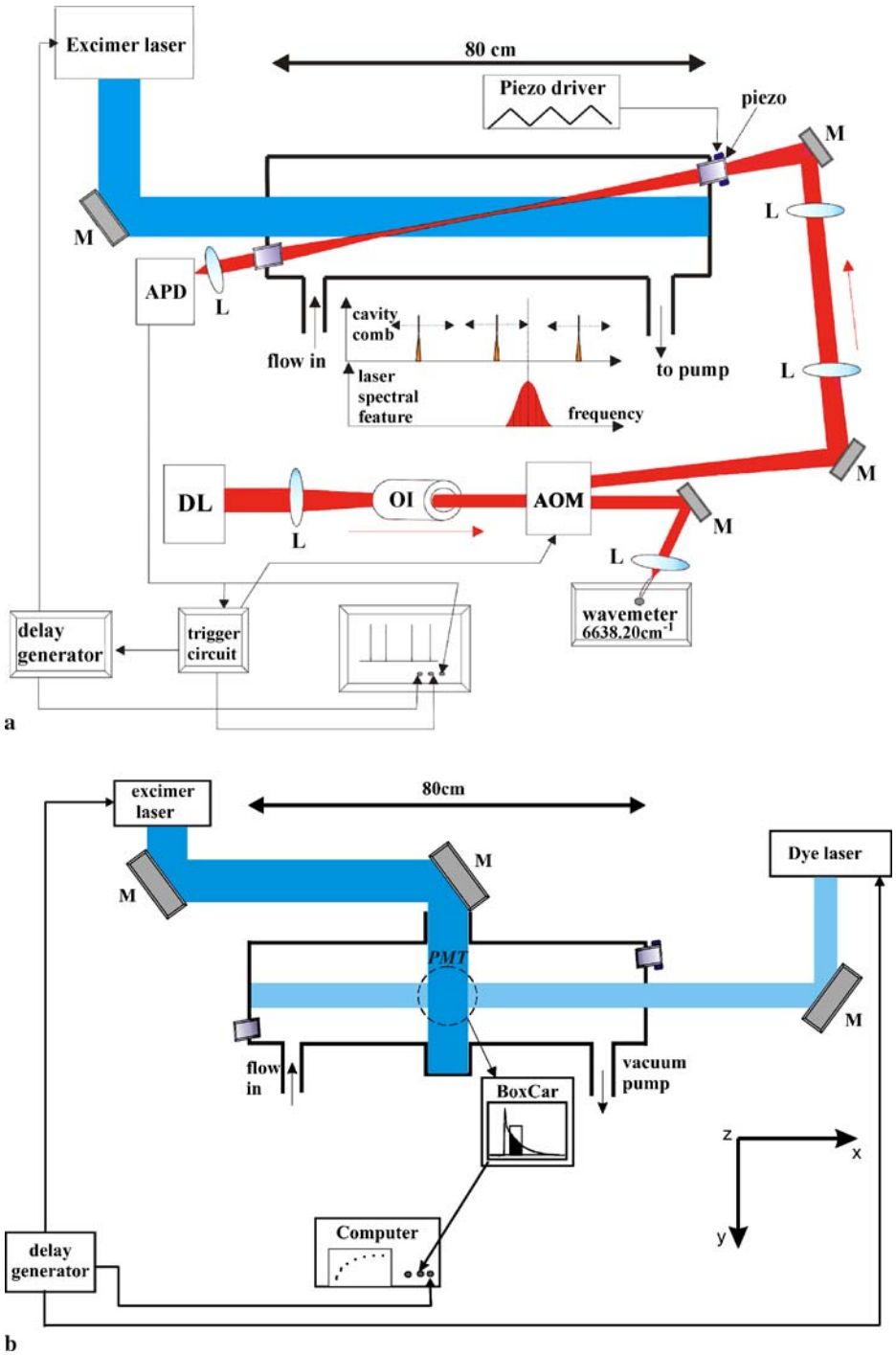

FIGURE 1 Schematic of the experimental set-up: (**a**) configuration for cw-CRDS measurements and (**b**) configuration for LIF measurements

lar to the gas flow (see Fig. 1b). Switching from one set-up to the other takes less than 30 min. The temperature of the gas mixtures was 296 ± 3 K in all experiments.

3 Results and discussion

In order to quantify the $HO_2^{\bullet}$ yield and to distinguish different processes possibly involved in its formation and consumption, several series of experiments have been performed by either LIF or cw-CRDS. All systems have been photolysed at 248 nm:

(a) $OH^{\bullet}$ concentration–time profiles in the system $H_2O_2/C_6H_6/He$ in order to verify the system by measuring pseudo-first order decays and comparing it with the well known rate constant for the reaction $C_6H_6 + OH^{\bullet}$.

(b) $OH^{\bullet}$ concentration–time profiles in the system H_2O_2/He in order to deduce the absolute H_2O_2 concentration by measuring pseudo-first order decays and using the well-known rate constant for the reaction $OH^{\bullet} + H_2O_2$.

(c) Absolute $HO_2^{\bullet}$ concentration–time profiles of the same system (H_2O_2/He) in order to obtain the initial absolute $OH^{\bullet}$ concentration for a given experimental condition (H_2O_2 concentration and laser fluence) from fitting

these profiles, assuming quantitative $HO_2^\bullet$ formation in the $OH^\bullet + H_2O_2$ reaction.

(d) Absolute $HO_2^\bullet$ concentration–time profiles in the system $C_6H_6/O_2/He$ allowing, by comparison with (c), to obtain relative initial $OH^\bullet$ and $HO_2^\bullet$ concentrations for a given H_2O_2 and C_6H_6 concentrations.

(e) Absolute $HO_2^\bullet$ concentration–time profiles in the system $C_6H_6/O_2/He$ with varying O_2 concentrations in order to reveal the origin of $HO_2^\bullet$.

(f) Absolute $HO_2^\bullet$ concentration–time profiles in the system $C_6H_6/H_2O_2/O_2/He$ in order to verify the conclusion from (d).

3.1 $OH^\bullet$ *profiles in the system* $H_2O_2/C_6H_6/He$: *(a) and (b)*

Three typical $OH^\bullet$ concentration–time profiles are shown in Fig. 2: the upper curve corresponds to the photolysis of 4.5×10^{14} cm^{-3} H_2O_2 only, for the two lower curves two different concentrations of C_6H_6 (0.7 and 1.4×10^{15} cm^{-3}) have been added. The fluorescence intensity is not an absolute technique, but these experiments have been performed one after the other, without changing any of the parameters linked to the fluorescence intensity like the high voltage applied to the photomultiplier, gate width or sensitivity of the boxcar, laser energies. Quenching of the $OH^\bullet$ fluorescence by the added C_6H_6 is also negligible in this concentration range. It can thus be deduced from Fig. 2 that the initial $OH^\bullet$ concentration is not influenced by the addition of C_6H_6. This is in contradiction to a former publication [10] where a linear increase in the $OH^\bullet$ concentration of up to a factor of 6 has been detected by continuous UV-laser absorption after addition of up to 3×10^{15} cm^{-3} C_6H_6. This observation has tentatively been explained in [10] by a photosensitized decomposition of H_2O_2 through excited C_6H_6. The interpretation was supported by the fact, that the addition of small amounts of O_2, a good quencher for excited C_6H_6, completely suppresses this phenomenon. No explanation can be given for this disagreement: the fact that we work in 6.6 kPa helium should increase this phenomenon, compared to the total pressure of 100 kPa N_2 in [10].

These experiments have been mainly performed in order to verify the system by measuring pseudo-first order decays and confirming the well known rate constant for the reaction of $C_6H_6 + OH^\bullet$ as well as to determine the H_2O_2 concentration in the photolysis cell by measuring pseudo-first order decays and using the well-known rate constant for the reaction $OH^\bullet + H_2O_2$.

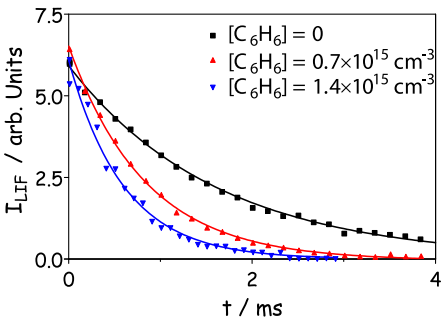

FIGURE 2 Time resolved LIF intensity from the photolysis of C_6H_6/H_2O_2 mixtures, $[H_2O_2] = 4.5 \times 10^{14}$ cm^{-3} for all three curves. No modification other than changing the C_6H_6 flow (high voltage of PM, gate settings or sensitivity for the boxcar, laser energy) has been done between the experiments, therefore the LIF intensity is proportional to the $OH^\bullet$ concentration: no change in $OH^\bullet$ fluorescence intensity has been observed by adding C_6H_6

3.2 $HO_2^\bullet$ *concentration–time profiles in the system* H_2O_2/He: *(c)*

A typical $HO_2^\bullet$ profile obtained after 248 nm photolysis of H_2O_2 is shown in Fig. 3. From a fit of this signal to the reaction scheme in Table 1 (only the reactions 4, 6, 7, 10 and 19 play a role in this system), using the well known rate constants, we are able to deduce initial OH-radical concentrations: in the example of Fig. 3 we found $[OH^\bullet]_0 = 1.6 \times 10^{12}$ cm^{-3} for an initial H_2O_2 concentration of 5×10^{14} cm^{-3}. Using an absorption cross section of 1×10^{-19} cm^2 [30] it can be calculated that a photolysis energy of 0.013 J cm^{-2} is necessary, in good agreement with the measured photolysis energy of 0.017 J cm^{-2} at the entrance of the reactor.

3.3 $HO_2^\bullet$ *concentration–time profiles in the system* C_6H_6/O_2: *(d)*

Figure 4 shows two $HO_2^\bullet$ profiles that have been obtained after photolysis of C_6H_6/O_2 in 6.6 kPa helium for two different C_6H_6 concentrations. We have no doubt that the observed signal proves the formation of HO_2 radicals, the detection by cw-CRDS is very selective and unambiguously: by scanning the wavelength we have verified that the absorption line is identical with the $HO_2^\bullet$ absorption line obtained by photolysing a $Cl_2/CH_3OH/O_2$ mixture. We have also verified that no signal remains when we turn off either the C_6H_6 or the O_2 flow. The full lines represent a simulation with the model from Table 1, most of the reactions and rate constants have been taken from [13]. In this system, the main reactions are 10, 11 and 12, only the rate constant for the reaction 11 ($C_6H_5O_2^\bullet + HO_2^\bullet$) has been adjusted to fit the decay. As can be seen, the agreement at short reaction times is very good, at longer reaction times the model slightly overestimates the $HO_2^\bullet$ consumption. Increasing the rate constant for reaction 12 will slow down the consumption, but even an unrealistic high rate constant of 4×10^{11} cm^3 s^{-1} does not perfectly fit the decays.

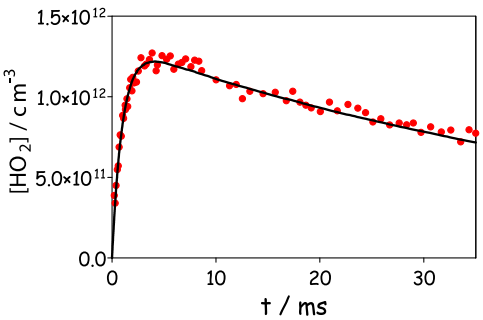

FIGURE 3 $HO_2^\bullet$ concentration–time profile obtained from the 248 nm photolysis of 5×10^{14} cm^{-3} H_2O_2 in 50 Torr He. $E_{248\,nm} = 0.013$ J cm^{-2}. *Full line* represents the mechanism from Table 1 with $[OH^\bullet]_0 = 1.6 \times 10^{12}$ cm^{-3}

No.	Reaction	k/cm^3 s^{-1}	Reference
1	$C_6H_6 \xrightarrow{h\nu_{248\,nm}} C_6H_6{}^*$		
2	$C_6H_6{}^* \rightarrow C_6H_6$	1.2×10^{6}[a]	This work
3	$C_6H_6{}^* + O_2 \rightarrow HO_2^\bullet + C_6H_5^\bullet$	1×10^{-10}	This work
4	$H_2O_2 \xrightarrow{h\nu} 2OH^\bullet$	$\varphi = 2$	[28]
5	$C_6H_5^\bullet + O_2 \rightarrow C_6H_5O_2^\bullet$	1.4×10^{-11}	[31]
6	$OH^\bullet + H_2O_2 \rightarrow HO_2^\bullet + H_2O$	1.7×10^{-12}	[30]
7	$OH^\bullet + HO_2^\bullet \rightarrow H_2O + O_2$	1.1×10^{-10}	[30]
8	$OH^\bullet + C_6H_6 \rightarrow C_6H_6OH^\bullet$	1.2×10^{-12}	[5]
9a	$C_6H_6OH^\bullet + O_2 \rightarrow C_6H_6OHO_2^\bullet$	1.25×10^{-16}	[13]
9b	$C_6H_6OH^\bullet + O_2 \rightarrow C_6H_5OH + HO_2^\bullet$	1.25×10^{-16}	[13]
10	$2HO_2^\bullet \rightarrow H_2O_2 + O_2$	1.7×10^{-12}	[30]
11	$HO_2^\bullet + C_6H_5O_2^\bullet \rightarrow$ products	4×10^{-11}	This work
12	$2C_6H_5O_2^\bullet \rightarrow$ products	1.6×10^{-12}	[13]
13	$2C_6H_6OH^\bullet \rightarrow$ products	4×10^{-11}	[13]
14	$C_6H_6OH^\bullet + OH^\bullet \rightarrow$ products	1×10^{-10}	[13]
15	$C_6H_6OH^\bullet + HO_2^\bullet \rightarrow$ products	5×10^{-11}	[13]
16	$C_6H_6OH^\bullet + RO_2^\bullet \rightarrow$ products	5×10^{-11}	[13]
17	$RO_2^\bullet + RO_2^\bullet \rightarrow$ products	1.6×10^{-12}	[13]
18	$RO_2^\bullet + HO_2^\bullet \rightarrow$ products	2×10^{-11}	[13]
19	$HO_2^\bullet \rightarrow$ diffusion	12[a]	This work
20	$C_6H_5O_2^\bullet \rightarrow$ diffusion	10[a]	This work

[a] Rate constant in s^{-1}, R = C_6H_6OH

TABLE 1 Reaction mechanism for analysis of experimental signals

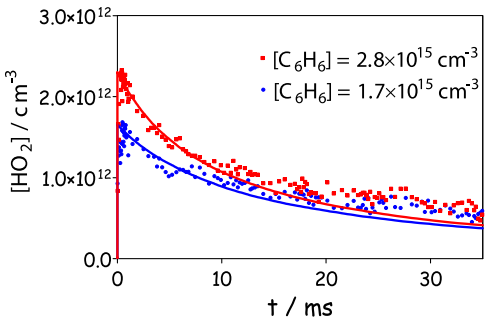

FIGURE 4 $HO_2^\bullet$ concentration–time profiles obtained from the 248 nm photolysis of 1.7 and 2.8×10^{15} cm^{-3} C_6H_6 in the presence of 1.4×10^{17} cm^{-3} O_2, photolysis energy is identical to those in Figs. 3 and 7, *full line* represents mechanism from Table 1 with $[C_6H_6{}^*]_0 = 1.7$ and 2.6×10^{12} cm^{-3}

The initial $C_6H_6{}^*$ concentration needed to reproduce the $HO_2^\bullet$ profiles increases linearly with the C_6H_6 concentration. With known laser fluence (the same as in Fig. 3: 0.013 J cm^{-2}, see above paragraph) and absorption cross section for C_6H_6 at 248.4 nm ($\sigma = 3.0 \times 10^{-19}$ cm^2) [U. Platt, private communication], we find a quantum yield of $\varphi = 0.2 \pm 0.1$ for the $HO_2^\bullet$ formation under our experimental conditions (6.6 kPa He, $[O_2] = 1.4 \times 10^{17}$ cm^{-3}), i.e. 20% of 248 nm photons absorbed by C_6H_6 lead to the formation of $HO_2^\bullet$.

The calculation of this quantum yield depends on the knowledge of all absorption coefficients (C_6H_6 at 248 nm and $HO_2^\bullet$ at 6638.20 cm^{-1}) as well as on the laser fluence (indirectly deduced under (c) using the absorption cross section of H_2O_2 at 248 nm). In order to bypass these uncertainties, we have directly compared the signals from Figs. 3 and 4: both have been done the same day one after the other, using the same laser fluence, alignment and diode laser wavelength. The H_2O_2 concentration has been obtained from the simulation of the signal in Fig. 3, i.e. the increase of $HO_2^\bullet$ governed by reaction 6, but also on other days by more precise OH-LIF measurements as seen in Fig. 2. From this simulation we obtain for the given laser fluence the ratio (see under (c)): $[OH^\bullet]_0/[H_2O_2] = 0.0032$. From the experiments in Fig. 4 we deduce for the same laser fluence a ratio of $[HO_2^\bullet]_0/[C_6H_6] = (0.0009 \pm 0.0002)$. Comparing these two ratios, we deduce that under our reaction condition, i.e. $[O_2] = 1.4 \times 10^{17}$ cm^{-3} in 6.6 kPa helium, the 248 nm excimer laser photolysis of equal amounts of H_2O_2 and C_6H_6 leads to initial radical concentrations of $[HO_2^\bullet]_0 = (0.28 \pm 0.05) \times [OH^\bullet]_0$. Please note, that this result depends only very little on the interpretation of the signals, i.e. on the reaction mechanism in Table 1 and on the rate constants therein. This result is also independent on any error in absorption cross sections, taken from the literature, on the photolysis laser energies or on the alignment geometry (error in the absorption path length [27]). But it should be noted that the C_6H_6 absorption spectrum is highly structured in this wavelength range, therefore the result will depend on the exact wavelength and bandwidth of the photolysis source (Lambda Physik LPX 202i, the emitted wavelength is 248.4 nm with a bandwidth of 0.8 nm) and care should be taken, when transferring the results from this work to other photolysis sources (Hg-lamps, for example).

As mentioned in the introduction, H_2O_2 photolysis at 248 nm has commonly been used [10, 12, 13, 24] to study the $OH^\bullet$ initiated oxidation of aromatic hydrocarbons. In order to privilege the reaction of OH radicals with C_6H_6 rather than with H_2O_2 (both rate constants are very similar), C_6H_6 has always been used in excess, sometimes up to a factor of 6 [10]. Under these conditions the initial $HO_2^\bullet$ concentration from excitation of C_6H_6 is twice as high as the $OH^\bullet$ concentration from the H_2O_2 photolysis. As a matter of course, there is a by-product to the HO_2 radical, probably $C_6H_5^\bullet$ getting possibly converted to $C_6H_5O_2$ radicals in the presence of O_2 [31]. These radicals can then influence the observed kinetics and it might be necessary to include them when analyzing the concentration–time profiles. It must be mentioned, that experiments in [10, 12] have been performed in 1 hPa N_2 which might have an influence on the $HO_2^\bullet$ quantum yield due to increased quenching of excited C_6H_6 (see Sect. 3.4): so far we have not performed any experiments on the pressure dependence of the $HO_2^\bullet$ yield.

3.4 *Absolute $HO_2^\bullet$ concentration–time profiles in the system $C_6H_6/O_2/He$ with varying O_2 concentrations: (e)*

The photolysis of C_6H_6 at 248 nm has been studied under collision free conditions using the molecular beam photofragmentation translational spectroscopy by Yokoyama et al. [32]. They find as products of this reaction only H_2 and $CH_3^\bullet$ with relative yields of 0.96 and 0.04, respectively, no information on the absolute yield has been given. The formation of H-atoms has been observed by these authors [32] after excitation with 193 nm only. Examination of the different energies demonstrates, that the C–H bond rupture should be slow: the 248 nm-photon energy of 481 kJ mol^{-1} faces an endothermicity of the C–H bond rupture of 463 kJ mol^{-1} [32].

It is thus not very likely that the observed HO_2 radicals originate from a direct reaction between O_2 and H-atoms. In order to confirm this, we have carried out a series of experiments with varying, low O_2 concentrations. In fact the rate constant of the reaction of H-atoms with O_2 is rather slow at our low pressure (3.7×10^{-14} cm^3 s^{-1} at 6.6 kPa Ar [33]), a decrease of $[O_2]$ would thus have a strong influence on the $HO_2^\bullet$ profile. In Fig. 5 are shown three $HO_2^\bullet$ profiles with varying, low O_2 concentrations ($0.7–1.8 \times 10^{16}$ cm^{-3}): under these conditions the pseudo-first order rate constant of the $H + O_2$ reaction would be on the order of a few 100 s^{-1}, which is visibly not in agreement with our observations, the O_2 concentration obviously does not influence the formation kinetic of $HO_2^\bullet$ (instantaneous on our time scale). However, the initial $HO_2^\bullet$ concentration decreases with decreasing O_2 concentration. Therefore, we have considered a reaction of excited $C_6H_6{}^*$ with O_2, leading to the formation of $HO_2^\bullet$ (instead of the commonly indicated quenching of the excited state) in parallel to a unimolecular relaxation:

$$C_6H_6 \xrightarrow{h\nu_{248\ \mathrm{nm}}} C_6H_6{}^* \quad \text{(R 1)}$$

$$C_6H_6{}^* \rightarrow C_6H_6 \quad \text{(R 2)}$$

$$C_6H_6{}^* + O_2 \rightarrow HO_2^\bullet + C_6H_5^\bullet\,. \quad \text{(R 3)}$$

A plot of $1/[HO_2^\bullet]_0$ as a function of $1/[O_2]$ in Fig. 6 shows good linearity for the signals from Fig. 5: the intercept of the regression line leads to $[C_6H_6{}^*]_0 = (3.6 \pm 1.2) \times 10^{12}$ cm^{-3}, the slope ($m = 3600 \pm 200$) leads to the ratio $k_2/k_3 = (1.2 \pm 0.6) \times 10^{16}$ cm^{-3}. The concentration of $C_6H_6{}^*$ can be compared to the number of absorbed photons: experiments in Fig. 5 have been conducted with $[C_6H_6] = 4.5 \times 10^{15}$ cm^{-3} and a photolysis energy of 0.014 J cm^{-2}, leading to a theoretical $[C_6H_6{}^*] = 1.6 \times 10^{13}$ cm^{-3}, i.e. a quantum yield of $\varphi = 0.23 \pm 0.04$ of the absorbed photons excite the state responsible for reaction 3. This result is in very good agreement with the yield $\varphi = 0.2$ obtained in paragraph (d).

The value of k_2/k_3 also seems reasonable: a probably rapid reaction with O_2 ($k_3 = 1 \times 10^{-10}$ cm^3 s^{-1}) leaves a rate of $k_2 = 1.2 \times 10^6$ s^{-1} for an O_2-independent relaxation process. This ratio also confirms our observations that initial $HO_2^\bullet$ concentrations do not change anymore within the experimental error at O_2 concentrations above 5×10^{16} cm^{-3}, i.e. k_2 becomes negligible compared to the pseudo-first order rate constant for reaction 3.

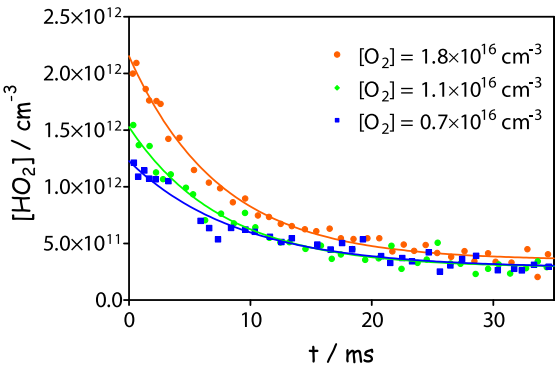

FIGURE 5 $HO_2^\bullet$ concentration–time profiles using different O_2 concentrations, $[C_6H_6] = 4.5 \times 10^{15}$ cm^{-3}, $E_{248\ \mathrm{nm}} = 0.014$ J cm^{-2}

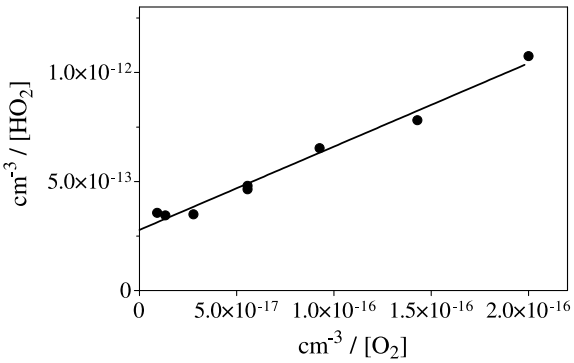

FIGURE 6 Plot of initial $1/[HO_2^\bullet]_0$ as a function of $1/[O_2]$ for concentration–time profiles as shown from Fig. 5

C_6H_6 in S_0 is excited by 248 nm photons into the $^1B_{2u}$ state of S_1, from where a rapid relaxation leads to vibrationally excited C_6H_6 in S_0^* [32]. The life time of the S_1 state is only $\tau = 28$ ns [34], it is therefore probable that reaction 3 involves vibrationally excited C_6H_6 rather than electronically excited C_6H_6 in S_1.

For the purpose of interpretation of our observations we have described the competing deactivation of $C_6H_6{}^*$ (R 2) as a unimolecular process. We have not yet performed experiments at different pressures or, even more interesting, in different bath gases. Hence, it is difficult to estimate if reaction 3 will be of importance in experiments conducted in 1 hPa N_2. Nevertheless, it is very interesting to notice, that Bohn and Zetzsch [10] mention an unexpected increase in $OH^\bullet$ concentration on the addition of C_6H_6, which they attribute to a benzene sensitised decomposition of H_2O_2. This increase in $OH^\bullet$ is suppressed by the addition of small amounts of O_2. Interestingly, the concentration of O_2 needed for this suppression, 0.3 kPa (6.8×10^{16} cm^{-3}), is very similar to the above mentioned concentration of 5×10^{16} cm^{-3}. It should thus not be ruled out, that formation of $HO_2^\bullet$ through (R 3) plays also a role at higher pressures.

3.5 $HO_2^\bullet$ *profiles in the system* $C_6H_6/H_2O_2/O_2$*: (f)*

We have finally added H_2O_2 to the reaction system from Fig. 4: the full lines in Fig. 7 show the simulations of the reaction scheme in Table 1, using as initial conditions the $OH^\bullet$ and H_2O_2 concentrations obtained from the simulation in Fig. 3 and the $HO_2^\bullet$ concentrations from Fig. 4. It can be seen, that the model reproduces very well the observed $HO_2^\bullet$ profiles at short reaction times, but at longer reaction times the model overestimates the $HO_2^\bullet$ consumption. The dashed line in Fig. 7 shows for comparison the decay expected for $HO_2^\bullet$ self-reaction and diffusion only, it is thus unequivocal that other reactions consume $HO_2^\bullet$. No attempts have been done in the frame of this work to adjust the model at longer reaction times, but it seems that some uncertainties persist in the model of Table 1 and more detailed experiments will be needed using a more extensive range of initial radical- and O_2 concentrations.

4 Conclusion

We have presented in this paper new experimental results regarding the oxidation mechanism of benzene C_6H_6

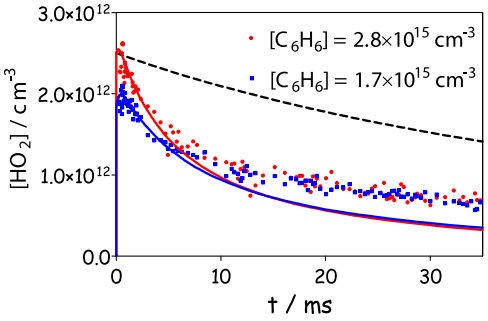

FIGURE 7 $HO_2^\bullet$ concentration–time profile obtained after addition of C_6H_6 (1.7 and 2.7×10^{15} cm^{-3}) and 1.4×10^{17} cm^{-3} O_2 to the reaction mixture from Fig. 3. *Full lines* represent the mechanism from Table 1 with $[C_6H_6{}^*]_0 = 1.7$ and 2.6×10^{12} cm^{-3} for the *lower* and *upper profiles*, respectively, photolysis energy is identical to those in Figs. 3 and 4. The *dashed line* shows the decay corresponding to $HO_2^\bullet$ self reaction and diffusion only

at low pressure. The direct formation of HO_2 radical from the 248 nm photolysis of C_6H_6 in the presence of O_2 has been detected without ambivalence. A quantum yield of $\varphi = 0.2 \pm 0.1$ for the $HO_2^\bullet$ formation has been deduced under our conditions ($[O_2] > 5 \times 10^{16}$ cm^{-3}, $p = 6.6$ kPa He). A comparison with $HO_2^\bullet$ profiles obtained from H_2O_2 photolysis has shown that, under these conditions, the 248 nm irradiation of equal initial concentrations of H_2O_2 and C_6H_6 lead to the following initial radical concentration: $[HO_2^\bullet]_0 = (0.28 \pm 0.05) \times [OH^\bullet]_0$. From experiments with varying O_2 concentrations the origin of the HO_2 radicals seems to be in a reaction between O_2 and excited C_6H_6. Earlier studies on the oxidation of C_6H_6 have frequently used the 248 nm photolysis of H_2O_2 to initiate the reaction sequence without taking into account this direct formation of $HO_2^\bullet$ for the interpretation. This might be a reason for the persisting discrepancy in the reaction mechanism, as the influence of this new aspect on interpretations and results will largely vary with the reaction conditions and also the detection technique.

ACKNOWLEDGEMENTS This work is financially supported by the Nord/Pas de Calais region within the framework of IRENI, by the CNRS, the European funds for Regional Economic Development FEDER. A. Aluculesei thanks the EU for financial support through the Marie Curie project EST-CT-2005-020659.

REFERENCES

1 R.G. Derwent, M.E. Jenkin, S.M. Saunders, M.J. Pilling, P.G. Simmonds, N.R. Passant, G.J. Dollard, P. Dumitrean, A. Kent, Atmosph. Environ. **37**, 1983 (2003)
2 R.A. Perry, R. Atkinson, J.N. Pitts, J. Phys. Chem. **81**, 296 (1977)
3 R. Knispel, R. Koch, M. Siese, C. Zetzsch, Ber. Bunsenges. Phys. Chem. **94**, 1375 (1990)
4 S.-C. Lin, T.-C. Kuo, Y.-P. Lee, J. Chem. Phys. **101**, 2098 (1994)
5 E. Bjergbakke, A. Sillesen, P. Pagsberg, J. Phys. Chem. **100**, 5729 (1996)
6 K. Lorenz, R. Zellner, Ber. Bunsenges. Phys. Chem. **87**, 629 (1983)
7 T.J. Wallington, D.M. Neuman, M.J. Kurylo, Int. J. Chem. Kinet. **19**, 725 (1987)
8 F. Witte, E. Urbanik, C. Zetzsch, J. Phys. Chem. **90**, 3251 (1986)
9 C.-C. Chen, T.H. Lay, J.W. Bozzelli, J. Phys. Chem. A **107**, 6451 (2003)
10 B. Bohn, C. Zetzsch, Phys. Chem. Chem. Phys. **1**, 5097 (1999)
11 R. Koch, R. Knispel, M. Elend, M. Siese, C. Zetzsch, Atmosph. Chem. Phys. **7**, 2057 (2007)
12 D. Johnson, S. Raoult, M.-T. Rayez, J.-C. Rayez, R. Lesclaux, Phys. Chem. Chem. Phys. **4**, 4678 (2002)
13 S. Raoult, M.-T. Rayez, J.-C. Rayez, R. Lesclaux, Phys. Chem. Chem. Phys. **6**, 2245 (2004)
14 S.Y. Grebenkin, L.N. Krasnoperov, J. Phys. Chem. A **108**, 1953 (2004)
15 T. Berndt, O. Boge, H. Herrmann, Chem. Phys. Lett. **314**, 435 (1999)
16 T. Berndt, O. Böge, Phys. Chem. Chem. Phys. **8**, 1205 (2006)
17 B. Klotz, I. Barnes, K.H. Becker, B.T. Golding, J. Chem. Soc. Faraday Trans. **93**, 1507 (1997)
18 R. Volkamer, B. Klotz, I. Barnes, T. Imamura, K. Wirtz, N. Washida, K.H. Becker, U. Platt, Phys. Chem. Chem. Phys. **4**, 1598 (2002)
19 B. Klotz, R. Volkamer, M.D. Hurley, M.P.S. Andersen, O.J. Nielsen, I. Barnes, T. Imamura, K. Wirtz, K.-H. Becker, U. Platt, T.J. Wallington, N. Washida, Phys. Chem. Chem. Phys. **4**, 4399 (2002)
20 W.A. Noyes, K.E. Al-Ani, Chem. Rev. **74**, 29 (1974)
21 C. Bloss, V. Wagner, M.E. Jenkin, R. Volkamer, W.J. Bloss, J.D. Lee, D.E. Heard, K. Wirtz, M. Martin-Reviejo, G. Rea, J.C. Wenger, M.J. Pilling, Atmosph. Chem. Phys. **5**, 641 (2005)
22 C. Bloss, V. Wagner, A. Bonzanini, M.E. Jenkin, K. Wirtz, M. Martin-Reviejo, M.J. Pilling, Atmosph. Chem. Phys. **5**, 623 (2005)
23 C.-C. Chen, J.W. Bozzelli, J.T. Farrell, J. Phys. Chem. A **108**, 4632 (2004)
24 B. Bohn, J. Phys. Chem. A **105**, 6092 (2001)
25 N. Ibrahim, J. Thiebaud, J. Orphal, C. Fittschen, J. Mol. Spectrosc. **242**, 64 (2007)
26 J. Thiebaud, C. Fittschen, Appl. Phys. B **85**, 383 (2006)
27 J. Thiebaud, S. Crunaire, C. Fittschen, J. Phys. Chem. A **111**, 6959 (2007)
28 J. Thiebaud, A. Aluculesei, C. Fittschen, J. Chem. Phys. **126**, 186 101 (2007)
29 E. Delbos, P. Devolder, L. ElMaimouni, C. Fittschen, K. Brudnik, J.T. Jodkowski, E. Ratajczak, Phys. Chem. Chem. Phys. **4**, 2941 (2002)
30 R. Atkinson, D.L. Baulch, R.A. Cox, J.N. Crowley, R.F. Hampson, R.G. Hynes, M.E. Jenkin, M.J. Rossi, J. Troe, Atmosph. Chem. Phys. **4**, 1461 (2004)
31 K. Tonokura, Y. Norikane, M. Koshi, Y. Nakano, S. Nakamichi, M. Goto, S. Hashimoto, M. Kawasaki, M.P. Sulbaek Andersen, M.D. Hurley, T.J. Wallington, J. Phys. Chem. A **106**, 5908 (2002)
32 A. Yokoyama, X. Zhao, E.J. Hintsa, R.E. Continetti, Y.T. Lee, J. Chem. Phys. **92**, 4222 (1990)
33 J. Hahn, L. Krasnoperov, K. Luther, J. Troe, Phys. Chem. Chem. Phys. **9**, 1997 (2004)
34 W. Hack, W. Langel, Il Nuovo Cimento B **63**, 207 (1981)